Q Control of an AFM Microcantilever with Double-Stack AlN Sensors and Actuators

Hazhir Mahmoodi Nasrabadi, Mohammad Mahdavi, *Member, IEEE*, and S. O. Reza Moheimani, *Fellow, IEEE*

***Abstract*— Active Atomic Force Microscope (AFM) cantilevers with integrated actuator/sensor pairs display larger feedthrough than conventional base excited cantilevers operating in conjunction with optical displacement sensors. To control the Q factor of a cantilever, this feedthrough needs to be canceled or significantly reduced. We use an AFM microcantilever with a double-stack sensor/actuator pair to address the feedthrough cancellation problem. Our device provides two sensor signals: one used for displacement sensing and the other for velocity measurement, with the latter being used for feedback. A readout circuit is designed to sense the displacement signal and to implement the velocity feedback controller. With this method, we were able to reduce the Q factor from 390 to 30.**

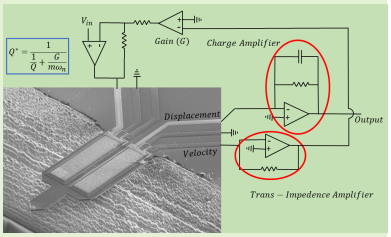

***Index Terms*— feedthrough cancellation, AFM, piezoelectric sensing/actuation, readout circuit, Q control**

I. Introduction

INTRODUCTION of Atomic Force Microscope (AFM) in 1986 [1] enabled unrivaled levels of performance in microscopy. For the past 35 years, atomic force microscope has been a major tool in scientific investigations at the nanoscale. The subnanometer resolution and the ability to operate in different environments have made the AFM a more attractive proposition than similar methods like Scanning Tunneling Microscopy (STM) and Scanning Electron Microscopy (SEM). The AFM collects data by scanning the sample surface with a sharp tip attached to the end of a microcantilever.

Several modes have been developed for AFM imaging, with the most common being: (i) contact mode, in which the tip and the sample are in contact throughout the scan; (ii) tapping mode, in which the tip and the sample are in intermittent contact; and (iii) non-contact mode, in which there is no contact between tip and sample. Measurements in contact mode imaging occur at low frequency. Thus, these measurements are affected by flicker noise [2] and are prone to low SNR. Continuous lateral forces acting on the sample from the probe tip [3] may cause wearing of the tip, image distortion, damage to delicate/soft samples, and displacement of weakly attached particles to the substrate. On the other hand, in ambient conditions, a thin layer of water may coat the surface of most samples, which may be several nanometers in thickness, dependent on the relative humidity. The non-contact mode requires that the tip must be kept close enough to the sample for interatomic forces to be detectable but far enough from the sample to avoid the tip from becoming stuck in the fluid layer due to the strong attractive capillary forces. A slower scan speed must be used for this reason.

Tapping mode combines the benefits of contact mode and non-contact mode, and it is more common, especially for delicate samples scanned in ambient conditions [4]. While the tip is intermittently contacting the sample surface during scanning, the cantilever experiences both repulsive and attractive forces; although, the average force is repulsive. This repulsive force changes the effective stiffness, and therefore, changes the cantilever's resonance frequency [4]–[6]. The effective Q factor will also be altered due to energy losses from the intermittent contact between tip and sample [7]. Variations of the cantilever resonance and Q factor lead to changes in the tip oscillation amplitude $A(t)$. This amplitude is commonly used to measure the tip-sample force, and consequently the sample topography, when imaging with a tapping-mode AFM.

In the conventional tapping mode AFM, the cantilever is actuated close to its first resonance frequency using a base shaker [8]. While oscillating, the tip strikes the sample once per cycle with a set amplitude. To measure the tip displacement, a light beam is reflected off the back of the cantilever onto a photodiode. The demodulated output signal of the photodiode is then used to determine the oscillation amplitude of the cantilever. As the cantilever scans the surface, the sample's topographic features alter the tip-sample force,

Manuscript received xx xx xxxx; revised xx xx xxxx; accepted xx xx xxxx. Date of publication xx xx xxxx; date of current version xx xx xxxx. Subject Editor xx xx xxxx. This work was supported by the U.S. Department of Energy's Office of Energy Efficiency and Renewable Energy (EERE) under the Advanced Manufacturing Office Award Number DEEE0008322. (Corresponding author: S. O. Reza Moheimani)

Hazhir Mahmoodi Nasrabadi and S. O. Reza Moheimani are with the Erik Johnsson School of Engineering and Computer Science, The University of Texas at Dallas, Richardson, TX 75080 USA (e-mail: hxm180003@utdallas.edu; reza.moheimani@utdallas.edu).

Mohammad Mahdavi was with Erik Johnsson School of Engineering and Computer Science, The University of Texas at Dallas, Richardson, TX, USA. He is now with Panasonic Corporation of North America, Marlborough, MA, USA. (e-mail: m.mahdavi@gmail.com)

leading to a change in resonance frequency and amplitude of oscillation. Due to the nonlinear nature of the tip-sample force [9], a feedback loop is needed to keep the oscillation amplitude constant. In this feedback loop, the error signal, which is the difference between the actual (A_0) and the desired (A_{set}) oscillation amplitudes, is fed into a PI controller. The control signal drives a Z positioner that adjusts the tip height so that the oscillation amplitude is kept constant. Since the position of the tip is changing according to the topography of the sample, the output of the PI controller represents the topography of the sample.

One of the problems in AFM is slow imaging. There has been, and still is, an on going effort to enable high-speed, and ultimately video-rate AFM imaging, which is necessary to capture the dynamics of biological processes [10]–[12]. These include increasing the cantilever resonance frequency [10], reducing the demodulator delay [13], increasing the Z-axis scanner bandwidth [14], [15], using alternative signals for topography estimation [16], [17], and reducing the cantilever Q factor. In many imaging applications, high scan speeds are desirable for better throughput [18] or to capture fast dynamic processes [19], [20]. In particular, controlling the Q factor of an AFM microcantilever has been an active research topic since its introduction in the early 1990s [21]. Increasing the Q factor of a cantilever will decrease the maximum force between tip and sample. Decreasing the Q factor, on the other hand, decreases the transient response of the microcantilever, which is a requirement in high-speed scans [22].

The basic approach to control the Q factor of a cantilever is to use the velocity signal in a negative feedback loop. However, in an AFM, we have access to the displacement signal, necessitating the estimation of the velocity signal from the displacement signal. Since the displacement signal is nearly sinusoidal, introducing a delay of $\pi/2\ rad$ at the resonance would serve as a simple velocity estimation. This method is commonly used in commercial AFMs. The issue, however, is that introduction of a delay into the feedback loop can cause instabilities due to the spill-over effect at high-frequency modes [23]–[26].

Some methods have been offered to address this issue. The observer-based control approach introduced in [27] uses a state observer and the knowledge of the system dynamics to estimate the cantilever's velocity signal from the displacement measurement. Other methods like resonant control [25] and piezoelectric shunt control [28], [29] make direct use of the displacement signal for feedback. A common feature of the cantilevers reported in the latter references is that they use actuators and sensors, micromachined on the tip-side of the device. These active cantilevers remove the need for a base shaker or an optical sensor. The compact size of these AFM cantilevers typically results in significant feedthrough from the actuation to the sensing signal [8]. Although the collocation of the sensor and the actuator is beneficial from a feedback control point of view, it tends to exacerbate this feedthrough problem. In a recent paper, we presented a new type of microcantilever with a pair of piezoelectric (AlN) sensors. This new microcantilever design exhibits a low feedthrough from actuation to sensing electrodes [30].

In this work, we propose a method to deal with the problem of high feedthrough levels in active microcantilevers with collocated sensing/actuation. This method uses our previously designed microcantilevers in [30] and provides direct access to both displacement and velocity signals at a low feedthrough level. It enables us to control the Q factor of the cantilever effectively. In section II, we briefly review the concept of the Q control as applied to AFM microcantilevers. In section III, the microfabrication steps are explained. Section IV describes the experimental implementation of the method and reports the results. Finally, section V concludes the paper.

II. Background and Theory

While scanning a surface in tapping mode, if there is a step in the topography that is faster than the rate of amplitude increment afforded by the feedback controller, the microcantilever will not be able to follow the topography. This is known as the "Parachuting" effect and is graphically depicted in Fig. 1 [4]. The cantilever loses contact with the surface, and since the amplitude of oscillation is set smaller than oscillation amplitude in the air ($Extended\ Factor = (A_{set}/A_{air}) < 1$), the oscillation amplitude increases to A_{air}. The controller adjusts the tip-surface distance to bring the oscillation amplitude back to the setpoint, A_{set}. During the transient response time, the amplitude changes as [31]:

$$A(t) = A_{set} + (A_0 - A_{set})(1 - e^{-\frac{\omega_n}{2Q}t}). \tag{1}$$

A_0 is the actual oscillation amplitude, ω_n is the resonance frequency, Q is the quality factor of the cantilever, and t is the time from when the parachuting starts. While the tip is in intermittent contact with the surface, the average tip-sample force is governed by [32]:

$$F_{TS} \propto \frac{k}{Q}\sqrt{A_0^2 - A_{set}^2}, \tag{2}$$

where k is stiffness of the cantilever.

Eq (1) implies that the smaller the Q factor, the faster the transient response of the cantilever and the shorter the probe loss. On the other hand, based on Eq (2), imaging with a low Q factor increases tip-sample force. A high tip-sample force can mechanically deform a soft sample resulting in a distorted image [33], [34]. Thus, one has to strike a compromise between the requirement to reduce the parachuting time and the desire to maintain a low tip-sample force.

One way to decrease the tip-sample force while lowering the Q factor is to maintain A_0 close to A_{set} as observed from Eq (2). However, doing this also reduces the amplitude of the error signal sent back to the Z-axis controller, which, upon encountering a sharp drop in the topography of the sample, increases the likelihood of losing contact between the tip and surface [35], [36]. Therefore, to have a high-quality image, there is a limitation on reducing the Q factor while also maintaining the tip-sample force in a reasonable amount to avoid sample deformation or tip corrosion. This limitation for our experiments is further discussed in the imaging results section.

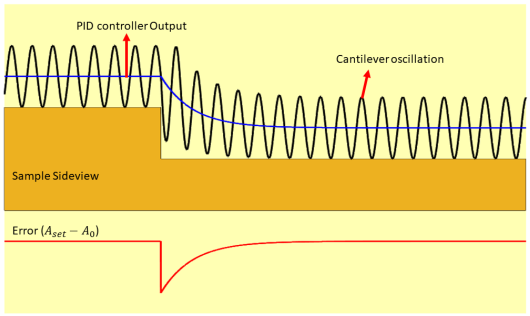

Fig. 1. Parachuting effect in AFM. After the oscillation amplitude increases because of the downward step in the sample topography, the Error signal ($\boldsymbol{Error} = \boldsymbol{A_{set}} - \boldsymbol{A_0}$) becomes negative. The PID controller compensates this negative error by bringing the tip and sample closer and decreasing the $\boldsymbol{A_0}$ to $\boldsymbol{A_{Set}}$.

Active Q control is straightforward if the velocity signal is available. The dynamics of the n^{th} resonance mode of a cantilever operating in the tapping mode can be described by the following differential equation:

$$m\ddot{d}(t) + \frac{m\omega_n}{Q}\dot{d}(t) + kd(t) = F_a cos(\omega_0 t) + F_{TS}(t). \quad (3)$$

m is the effective mass of the cantilever, and d is the tip displacement from its neutral position in the z direction. Two external forces are $F_a cos(\omega_0 t)$, which is the driving force, and F_{TS}, which is the tip-sample force.

If the cantilever's velocity signal is amplified (G), fed back, and combined with the driving force, Eq (3) can be rewritten as:

$$m\ddot{d}(t) + \frac{m\omega_n}{Q}\dot{d}(t) + kd(t) = F_a cos(\omega_0 t) + F_{TS}(t) - G\dot{d}(t), \quad (4)$$

which can be further simplified as:

$$m\ddot{d}(t) + \frac{m\omega_n}{Q^\star}\dot{d}(t) + kd(t) = F_a cos(\omega_0 t) + F_{TS}(t), \quad (5)$$

where

$$Q^\star = \frac{1}{\frac{1}{Q} + \frac{G}{m\omega_n}} \quad (6)$$

Eq (6) suggests that by changing the feedback gain, G, the effective Q factor of the cantilever can be changed arbitrarily. Thus, the problem of the Q control boils down to feeding back the velocity signal and subtracting it from the actuation signal.

The actuation/sensing design used in this paper enables two sensing output signals with low feedthrough levels. These two signals have 180° phase difference [30]. Our designed readout circuit achieves the above-mentioned purposes. It controls the Q factor by feeding back one of the sensing signals as the velocity signal, multiplying it with a feedback gain, and combining it with the input signal. The circuit amplifies the second signal to measure the displacement signal. The circuit design will be further explained in section IV-A, and the experimental results are presented in section IV-B.

III. Fabrication Process

Several methods have been proposed for on-chip actuation and sensing of AFM microcantilevers, see [37], [38], and [39]. Since we require two output signals, we can use active cantilevers with more than one sensing outputs, e.g. differential sensing designs. Among such sensing designs, [30] has the lowest feedthrough from the actuation electrode to the sensing electrodes. The connection of the actuation and the sensing electrodes are as illustrated in Fig. 5.

Each stack is comprised of layers of Molybdenum (Mo), Aluminium Nitride (AlN), Molybdenum (Mo), Aluminium Nitride (AlN), and Al (Aluminium) as the bottom electrode, the bottom piezoelectric material, the middle electrode, the top piezoelectric material, and the top electrode, respectively. The initial wafer for the microfabrication process is an SOI 100 silicon wafer with a $400\mu m$ handle layer, a $1\mu m$ buried oxide, and a highly doped $5\mu m$ device layer. The detailed process flow is sketched in Fig. 2.

The process starts with growing $500nm$ thermal oxide (Fig. 2(a)) on the device layer. This layer isolates the device layer from signal tracks and the bottom electrode. After this step, 4 layers of Mo($200nm$), AlN($1\mu m$), Mo($200nm$), and AlN($1\mu m$) are deposited consecutively, (Fig. 2(b)). These four layers are patterned from the top AlN layer to the bottom Mo layer, respectively (Fig. 2(c) to 2(f)). Patterning of each layer starts with depositing $200nm$ Silicon Oxide with the Plasma Enhanced Chemical Vapor Deposition (PECVD) process as a sacrificial hardmask. Following a lithography process with the SPR220-3 photoresist, the oxide layer is etched with a Reactive Ion Etching (RIE) recipe consisting of CHF3/Ar plasma.

The top AlN layer is etched by a Chlorine-based plasma (Fig. 2(c)), followed by a 10 to 20 seconds wet etch of AlN by tetramethylammonium hydroxide (TMAH). TMAH wet etch does not etch through Mo. Thus, it is ideal for removing the residues of the AlN layer left on the Mo layer (the middle electrode). Prior to starting the patterning of the next layer, the photoresist is stripped by acetone, and the hardmask is removed by wet etch BOE.

After the oxide deposition and the lithography, and once the oxide hardmask is etched, Mo (the middle layer) is etched with the same Chlorine-based plasma that was used for the AlN etch (Fig. 2(d)). This step is followed by cleaning the photoresist with acetone and then removing the hardmask with wet etch BOE. For the next AlN/Mo (bottom piezoelectric/bottom electrode) layers, the same deposition, patterning, etching, and removing steps are performed (Fig. 2(e), 2(f)).

Following the above steps of patterning all the layers, and before the deposition of the top electrode, we deposit a $500nm$ layer of Silicon Oxide. This oxide layer provides a spacer to avoid a short between the top electrode and the other metal layers (the middle and the bottom electrodes). The remainder of this layer is etched from the top of the transducers and vias. Through small openings carved into the oxide layer, electrical connections from the top electrode to the middle

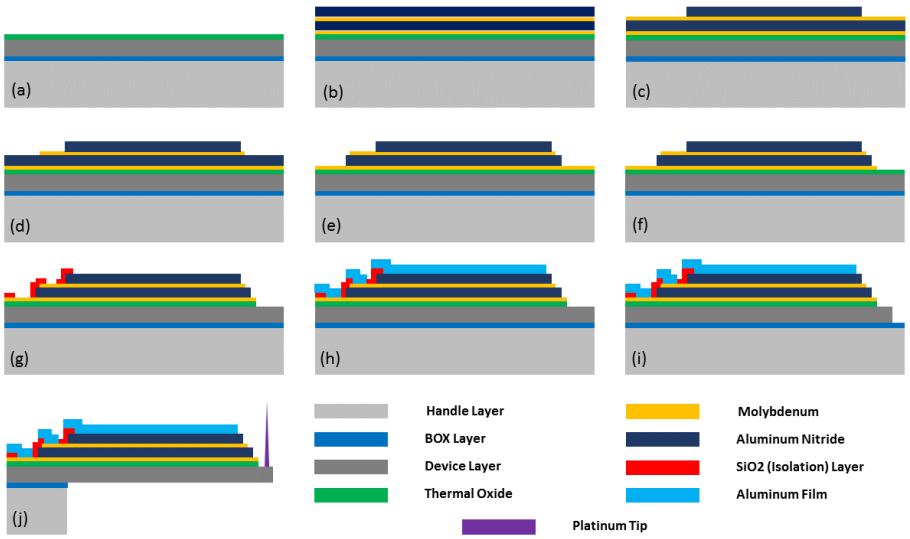

Fig. 2. Microfabrication process steps of a cantilever with a two-layer stack transducer (cross-sectional view). (a) Thermal oxide growth, (b) Deposition of Mo/AlN/Mo/AlN layers, (c) Shaping the top piezoelectric transducer, (d) Shaping the middle electrode, (e) Shaping the bottom piezoelectric transducer, (f) Shaping the bottom electrode, (g) Second oxide isolation deposition and etching, (h) Top electrode lift-off process, (i) Shaping microcantilever's body (Device Layer), and (j) Releasing the microcantilevers and depositing the Pt tip with FIB tool.

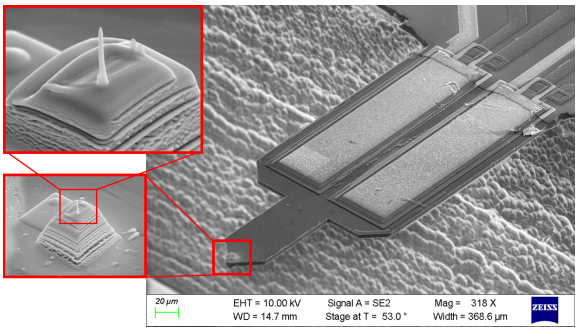

Fig. 3. The SEM image of the microfabricated cantilever.

and the bottom electrodes are provided (Fig. 2(g)). Then the photoresist is stripped, and the wafer is cleaned and prepared for the top layer (Al) deposition.

In order to avoid a reaction between the top AlN layer and the photoresist developer during the lift-off process (see Fig. 2(g)), we need to protect the AlN layer with a $100nm$ sacrificial layer of PECVD oxide prior to the lithography. Once a layer of photoresist is patterned for the lift-off of the top electrode (Al), this sacrificial oxide layer is wet etched with BOE 20:1 and then $1\mu m$ Al is deposited by an e-gun evaporator machine. To lift the Al layer off, the wafer is kept in acetone overnight (Fig. 2(h)).

The cantilever body is then defined by a designed mask and through Deep Reactive Ion Etching (DRIE) (Fig. 2(i)) of the $5\mu m$ device layer. To mechanically protect the front-side of the wafer during the backside DRIE process, a $1\mu m$ thick layer of Parylene is deposited on the front-side of the wafer. For the last $100\mu m$ of the backside DRIE process, the wafer is diced into smaller parts. The etching of each slice is continued on a carrier wafer. At this step, the $1\mu m$ buried oxide layer is etched with CHF3/Ar plasma, and the cantilever is released. As the final step, and after cleaning cantilevers with oxygen plasma, a nanoscale sharp Platinum tip is deposited using an FEI Nova 200 Focused Ion Beam (FIB) tool (Fig. 2(j)). We first deposit the base for the tip using Ion beam platinum depositor. We narrow down the deposition area for every $200\,nm$ of deposition so that the base looks like a pyramid structure. This trick narrows the tip base down and helps to reduce the unwanted forces between the tip base atoms and the sample atoms, while imaging. The very end of the tip sits on top of this base structure (see Fig. 3). To secure a very sharp tip, this part is deposited with the minimum deposition area for $20\,s$. The overall length of the tip, including the base, is $6\mu m$ and the radius of the very end of the tip is about $50nm$. Fig. 3 shows the SEM image with more details of the final device.

IV. Experimental Results

As discussed in Section II, one approach to control the Q factor of cantilevers is based on the velocity feedback, whereby the velocity signal is measured, multiplied in gain, and subtracted from the actuation voltage. In this section, we first describe the readout circuit. Then we investigate the cantilever's frequency response for different velocity feedback gains. In the end, we provide the imaging results for two Q factors of the same cantilever.

A. Readout Circuit

In order to measure the displacement signal, the top electrode voltage signal passes through a charge amplifier, which is shown in Fig. 5 as CA. The output of the charge amplifier is:

$$V_{out} = -\frac{j\omega R_{f_2}}{1 + j\omega R_{f_2} C_{f_2}} Q_T. \tag{7}$$

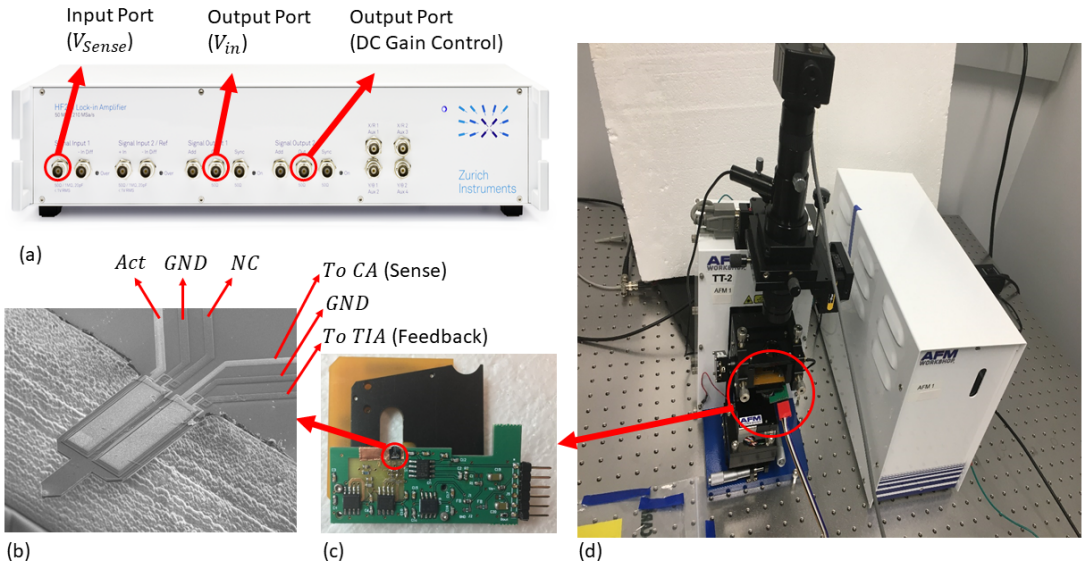

Fig. 4. The complete AFM imaging setup including: (a) the Lock-In Amplifier, (b) The active microcantilever with a double-stack sensing/actuation design, (c) The cantilever mounted on the readout PCB (the board is loaded on a custom designed cantilever holder), and (d) TT-2 AFM setup.

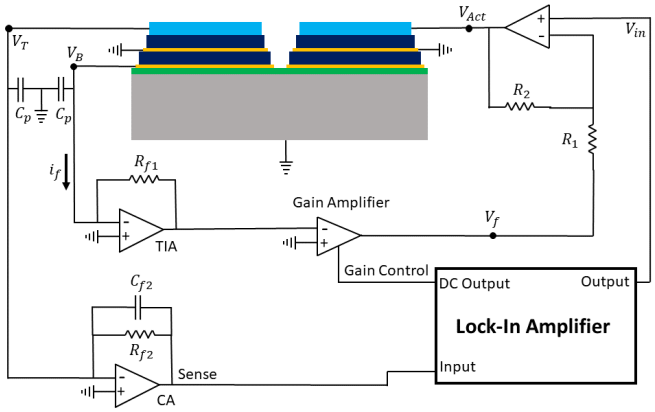

Fig. 5. Schematic of the device including its readout circuit that measures the displacement signal with a Charge Amplifier (CA stage) and produces the velocity signal with a Trans-Impedance Amplifier (TIA stage). The velocity signal is then multiplied with a gain (Gain Amplifier), that is then subtracted from the input signal.

$C_{f_2} = 0.2pF$ and Q_T is the generated charge by the top piezoelectric layer. For a large R_{f_2} (here, $500M\Omega$), $V_{out} \approx -(1/C_{f_2})Q_T$. The circuit functions as a high-pass filter with a corner frequency of $f_c = 1/(2\pi R_{f_2} C_{f_2})$. The large R_{f_2} results in a relatively low corner frequency, which is desirable in order to avoid signal attenuation at resonance.

The current signal produced by the bottom electrode charge (Q_B), which is:

$$i_f = j\omega Q_B, \tag{8}$$

is passed through a trans-impedance amplifier followed by a variable gain amplifier to produce the feedback voltage (V_f):

$$V_f = j\omega G R_{f_1} Q_B. \tag{9}$$

$R_{f_1} = 500k\Omega$ and G is the gain of the variable gain amplifier, which controls the cantilever's Q factor (see Eq 6).

Since $Q_T = -Q_B$ [30], from (7) and (9), it can be observed that:

$$V_f = j\omega G R_{f_1} C_{f2} V_{out}, \tag{10}$$

and in time domain:

$$V_f = G R_{f_1} C_{f2} \dot{V}_{out}. \tag{11}$$

Eq (11) shows that V_f is proportional to the derivative of V_{out} ($V_f \propto dV_{out}/dt$). Since V_{out} represents the displacement signal, V_f signal corresponds to the velocity of the cantilever oscillation ($\nu = \dot{x}$). Contrary to time delay active Q controller [22], current method works for all types of signals and not just sinusoidal inputs.

The actuation signal is obtained by subtracting V_f from V_{in}, i.e.

$$V_{Act} = (1 + \frac{R_2}{R_1})V_{in} - \frac{R_2}{R_1}V_f, \tag{12}$$

where $R_1 = R_2 = 1k\Omega$.

Eq (11) shows that the velocity signal has a positive gain, and thus, in (6), the gain (G) is positive. Therefore, this method only can decrease the Q factor. A non-inverting gain amplifier can increase the Q factor.

To properly characterize the circuit, we need to measure the actuation gain of the cantilever and the deflection sensitivity of the circuit. First, the gain of the gain amplifier is set to $-40\,dB$, which results in negligible velocity feedback, thus a nearly open-loop system. Therefore there is no Q control. Then, the cantilever's tip displacement is measured by a Polytech MSA-100 Laser Doppler Vibrometer (LDV). Applying a $200\,mv_{pp}$ voltage to the actuation electrode

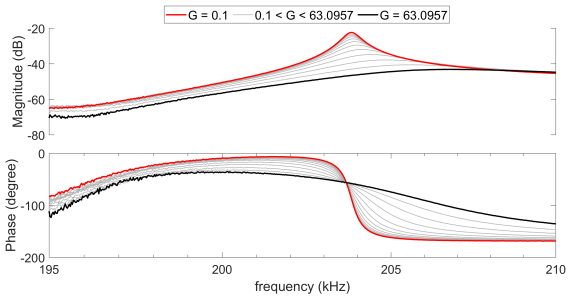

Fig. 6. Frequency Response of the Cantilever with different gains for velocity signal. Gain varies from **0.1** (red) to almost **63** (Black)

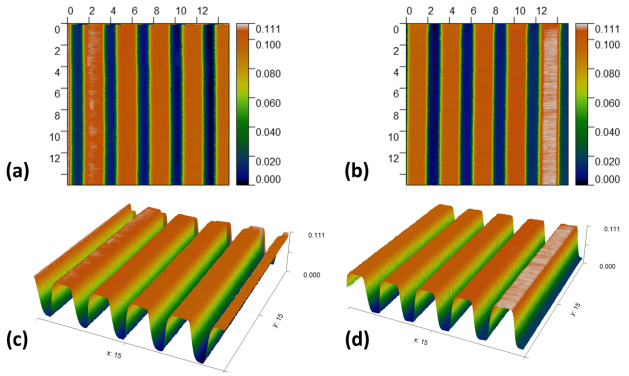

Fig. 7. (a) 2D topography with High Q. (b) 2D topography with Low Q. (c) 3D topography with High Q. (d) 3D topography with Low Q.

results in a displacement of $129.5\,nm_{pp}$ and a circuit output signal of $92.75\,mv_{pp}$. These measurements show that the deflection sensitivity of the sensing mechanism for the first mode of oscillation is $0.7162\,mv/nm$ and the actuation gain of the device is $0.6475\,nm/mV$. These data show a good agreement with the reported results by Mahdavi *et al.* in [26]. In that design, since the actuation and the sensing electrodes cover the entire cantilever surface, the deflection sensitivity and the actuation gain are almost twice the numbers in this report. The very small difference arises from the imperfect microfabricated device and also the imperfect electronic components of the PCB.

B. Frequency response

The cantilever is mounted on and wire-bonded to the readout circuit to apply the actuation signal and read out the sensing signals. Oscillator output from a Lock-In Amplifier (LIA) (HF2LI Zurich Instruments) is fed as a sine actuation voltage to the circuit (V_{in}), and the circuit output voltage (V_{out}) is delivered to the input port of the LIA. The input voltage (V_{in}) excites the cantilever at its first resonance frequency of $202.1kHz$. Fig. 4 illustrates the connections to the cantilever and the LIA.

The Gain Amplifier used in the circuit is VCA810, which, by changing the DC voltage applied to its gain control pin (see Fig. 5), the gain of the amplifier varies from $-40\,dB$ to almost $+40\,dB$. This gain change controls the velocity feedback gain, and thus, the Q factor of the cantilever. The result of the Q control can be observed in Fig. 6, where the Q factor changes from 392 (with $G = 0.1$) to 30 (with $G \approx 63.1$).

Since the sensing and the actuation electrodes are located in different transduction stacks (see Fig. 5), in theory, the feedthrough level should be zero. However, in practice, the adjacency of the two stacks and the low distance between sensing and actuation tracks introduce some feedthrough to the system. This effect can be observed in Fig. 6, and is visible at frequencies below $197\,kHz$.

C. Imaging Results

We performed tapping mode AFM imaging at the 1^{st} mode of the cantilever to capture the topographic profile of NT-MDT TGZ 110 calibration grating with sample heights of $110 \pm 2\,nm$. The grating features repeating rectangular steps with a period of $3.00 \pm 0.05\,\mu m$. Prior to imaging, the piezoelectric actuator is excited to reach the displacement amplitude of $\sim 259\,nm$, validated earlier by the Laser Doppler Vibrometer (LDV). Using the automated approach feature of the commercial AFM, the cantilever is brought into intermittent contact with the surface. It is then raster scanned over the calibration grating with the scan area set to $15 \times 15\,\mu m^2$. The obtained 2D and 3D images of the calibration grating are post-processed by Gwyddion software's standard built-in tools, such as mean plane subtraction, row alignment, and polynomial background removal.

As illustrated in Fig. 4(b) and 4(c), the microcantilever is wire-bonded to a readout circuit and mounted on a custom-designed cantilever holder that is then integrated into an AFMWorkshop TT-AFM. The input channel 1 of the LIA is used for sensing, the output channel 1 is used for actuation, and the output channel 2 produces the DC voltage, which controls the gain of the velocity feedback signal. The complete setup and the LIA connections are shown in Fig. 4(a) and 4(d).

As the scan rate increases, the slow transient response of the cantilever becomes an issue, necessitating active Q-control to enable high-speed tapping mode imaging. Scans were performed at the rate of $2\ rows/s$. With each row being $15\mu m$ long, this means a scan speed of $30\mu m/s$. For a very low feedback gain (almost without Q control), the cantilever features a high Q factor of 390. Since

$$BW_{3dB} = \frac{f_{res}}{Q}, \tag{13}$$

a bandwidth of $518Hz$ is feasible. Such a narrow bandwidth slows down the transient response of the closed-loop imaging system, leading to parachuting effect and making it difficult to capture step-like features on the topography shown in Fig. 7(a) and 7(c). Decreasing the Q factor to below 80, resulted in high tip-sample force and therefore image artifacts. Thus, Q factor of ~ 90 is chosen for low Q factor imaging, which results in a bandwidth of $BW_{3dB} \approx 2253Hz$ and improved imaging conditions, as seen in Fig. 7(b) and 7(d).

It is important to note that similar results could not be obtained without Q control through increasing the gain of the controller. The PI tracking controller was tuned, without Q control, by increasing its gain. The tuning led to proportional

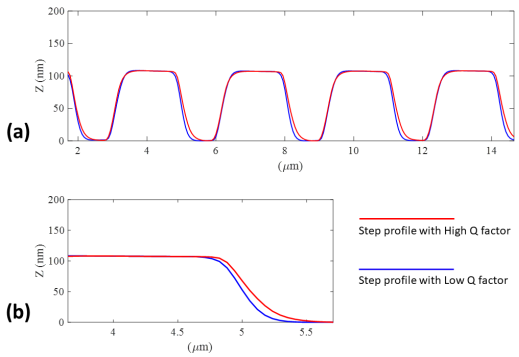

Fig. 8. (a) Cross-section of 3D topography of the sample, scanned with high Q (blue) and low Q (red) factors, (b) Zoomed in view of the step profile

and integral gains of 2 and 4000, respectively. These parameters result in the highest possible closed loop bandwidth, and thus the highest scan speed results with no Q control. However, this high bandwidth is achieved at the cost of very low stability margins, due to the high gain of the controller and the high the Q factor of the system. In the interest of making a fair comparison, we applied identical control parameters to the Q controlled cantilever. Lowering the Q factor of the cantilever reduces the gain at resonance, resulting in higher stability margins, with the same controller, in addition to improving the probe loss. Higher stability margins allow us to operate the tracking controller gains, if needed.

To better appreciate the improvement achieved by transitioning from low to high Q factor, the cross-sections of the two topographies are compared in Fig. 8.

V. Conclusion

The relatively high Q factor of the AFM cantilever limits the achievable scan speed in tapping-mode AFM. Being able to actively control the Q factor by taking advantage of on-chip sensors and actuators is a significant stepping stone to achieving high-speed on-chip AFM. In this work, we demonstrated how the velocity feedback control technique could be applied to a custom-designed active microcantilever with a simple electronic circuit. The design minimizes actuator-to-sensor feedthrough by separating actuation and sensing electrodes. Integration of the cantilever with the readout circuit on the same PCB enables us to capture velocity and displacement signals separately, and control the Q factor of the cantilever with the velocity signal feedback technique. We demonstrated that the Q factor of the cantilever could be changed and showed its effect on the accuracy of topographic features acquired in tapping mode AFM.

Acknowledgment

The authors would like to thank Nastaran Nikooienejad for assisting in the AFM image processing, Afshin Alipour for assisting with FIB tip deposition, and Emma Fowler for helping with editing the paper. They also would like to thank cleanroom staff at The University of Texas at Dallas.

References

[1] G. Binnig, C. F. Quate, and C. Gerber, "Atomic Force Microscope," *Phys. Rev. Lett.*, vol. 56, pp. 930–933, Mar 1986.

[2] S. M. Salapaka and M. V. Salapaka, "Scanning Probe Microscopy," *IEEE Control Systems Magazine*, vol. 28, no. 2, pp. 65–83, 2008.

[3] Q. Zhong, D. Inniss, K. Kjoller, and V. Elings, "Fractured polymer/silica fiber surface studied by tapping mode atomic force microscopy," *Surface Science Letters*, vol. 290, no. 1-2, pp. L688–L692, 1993.

[4] M. W. Fairbairn and S. O. R. Moheimani, "Control techniques for increasing the scan speed and minimizing image artifacts in tapping mode atomic force microscopy: Toward video-rate nanoscale imaging," *IEEE Control Systems Magazine*, vol. 33, no. 6, pp. 46–67, 2013.

[5] R. Garcıa and R. Perez, "Dynamic atomic force microscopy methods," *Surface science reports*, vol. 47, no. 6-8, pp. 197–301, 2002.

[6] A. Humphris, J. Tamayo, and M. Miles, "Active quality factor control in liquids for force spectroscopy," *Langmuir*, vol. 16, no. 21, pp. 7891–7894, 2000.

[7] J. Tamayo, "Study of the noise of micromechanical oscillators under quality factor enhancement via driving force control," *Journal of applied physics*, vol. 97, no. 4, p. 044903, 2005.

[8] S. Belikov, J. Alexander, M. Surtchev, and S. Magonov, "Digital Q-Control and automatic probe landing in amplitude modulation phase imaging AFM mode," *IFAC-PapersOnLine*, vol. 50, no. 1, pp. 10882–10888, 2017. 20th IFAC World Congress.

[9] S. Eslami and N. Jalili, "A comprehensive modeling and vibration analysis of AFM microcantilevers subjected to nonlinear tip-sample interaction forces," *Ultramicroscopy*, vol. 117, pp. 31–45, 2012.

[10] M. Viani, T. Schäffer, G. Paloczi, L. Pietrasanta, B. Smith, J. Thompson, M. Richter, M. Rief, H. E. Gaub, K. W. Plaxco, *et al.*, "Fast imaging and fast force spectroscopy of single biopolymers with a new atomic force microscope designed for small cantilevers," *Review of Scientific Instruments*, vol. 70, no. 11, pp. 4300–4303, 1999.

[11] A. Humphris, M. Miles, and J. Hobbs, "A mechanical microscope: High-speed atomic force microscopy," *Applied physics letters*, vol. 86, no. 3, p. 034106, 2005.

[12] T. Ando, "High-speed atomic force microscopy coming of age," *Nanotechnology*, vol. 23, no. 6, p. 062001, 2012.

[13] D. Y. Abramovitch, "Low Latency Demodulation for Atomic Force Microscopes, Part I Efficient Real-Time Integration," in *Proceedings of the 2011 American Control Conference*, pp. 2252–2257, IEEE, 2011.

[14] Y. K. Yong and S. O. R. Moheimani, "Collocated Z-axis Control of a High-Speed Nanopositioner for Video-Rate Atomic Force Microscopy," *IEEE Transactions on Nanotechnology*, vol. 14, no. 2, pp. 338–345, 2015.

[15] C. Lee and S. M. Salapaka, "Fast imaging with alternative signal for dynamic atomic force microscopy," *Applied Physics Letters*, vol. 97, no. 13, p. 133101, 2010.

[16] A. Bazaei, Y. K. Yong, and S. O. R. Moheimani, "Combining Spiral Scanning and Internal Model Control for Sequential AFM Imaging at Video Rate," *IEEE/ASME Transactions on Mechatronics*, vol. 22, no. 1, pp. 371–380, 2017.

[17] D. R. Sahoo, A. Sebastian, and M. V. Salapaka, "Transient-signal-based sample-detection in atomic force microscopy," *Applied Physics Letters*, vol. 83, no. 26, pp. 5521–5523, 2003.

[18] Borionetti, G., Bazzali, A., and Orizio, R., "Atomic force microscopy: A powerful tool for surface defect and morphology inspection in semiconductor industry," *Eur. Phys. J. Appl. Phys.*, vol. 27, no. 1-3, pp. 101–106, 2004.

[19] T. Ando, N. Kodera, Y. Naito, T. Kinoshita, K. Furuta, and Y. Y. Toyoshima, "A High-Speed Atomic Force Microscope for Studying Biological Macromolecules in Action," *ChemPhysChem*, vol. 4, no. 11, pp. 1196–1202, 2003.

[20] N. Kodera, D. Yamamoto, R. Ishikawa, and T. Ando, "Video imaging of walking myosin V by high-speed atomic force microscopy," *Nature*, vol. 468, no. 7320, pp. 72–76, 2010.

[21] J. Mertz, O. Marti, and J. Mlynek, "Regulation of a microcantilever response by force feedback," *Applied Physics Letters*, vol. 62, no. 19, pp. 2344–2346, 1993.

[22] H. Hölscher and U. D. Schwarz, "Theory of amplitude modulation atomic force microscopy with and without Q-Control," *International Journal of Non-Linear Mechanics*, vol. 42, no. 4, pp. 608 – 625, 2007. Special Issue Micro-and Nanoscale Beam Dynamics.

[23] M. Balas, "Feedback Control of Flexible Systems," *IEEE Transactions on Automatic Control*, vol. 23, no. 4, pp. 673–679, 1978.

[24] R. W. Stark, "Time Delay Q-Control of the Microcantilever in Dynamic Atomic Force Microscopy," in *5th IEEE Conference on Nanotechnology, 2005.*, pp. 259–262, IEEE, 2005.
[25] M. Fairbairn and S. O. R. Moheimani, "Resonant control of an atomic force microscope micro-cantilever for active Q control," *Review of Scientific Instruments*, vol. 83, no. 8, p. 083708, 2012.
[26] M. Mahdavi, H. M. Nasrabadi, M. Soleymaniha, and S. O. R. Moheimani, "Modal Actuation and Sensing with an Active AFM Cantilever," *IEEE Sensors Journal*, 2021.
[27] D. R. Sahoo, T. De Murti, and V. Salapaka, "Observer based imaging methods for Atomic Force Microscopy," in *Proceedings of the 44th IEEE Conference on Decision and Control*, pp. 1185–1190, IEEE, 2005.
[28] M. W. Fairbairn, S. O. R. Moheimani, and A. J. Fleming, "Q Control of an Atomic Force Microscope Microcantilever: A Sensorless Approach," *IEEE/ASME Journal of Microelectromechanical Systems*, vol. 20, no. 6, pp. 1372 – 1381, 2011.
[29] M. W. Fairbairn, P. Müller, and S. O. R. Moheimani, "Sensorless Implementation of a PPF Controller for Active *Q* Control of an AFM Microcantilever," *IEEE Transactions on Control Systems Technology*, vol. 22, no. 6, pp. 2118–2126, 2014.
[30] M. Mahdavi, M. B. Coskun, H. M. Nasrabadi, and S. O. R. Moheimani, "A high dynamic range AFM probe with collocated piezoelectric transducer pairs," in *The 33rd IEEE International Conference on Micro Electro Mechanical Systems (MEMS 2020)*, 2020.
[31] T. Sulchek, G. G. Yaralioglu, C. F. Quate, and S. C. Minne, "Characterization and optimization of scan speed for tapping-mode atomic force microscopy," *Review of Scientific Instruments*, vol. 73, no. 8, pp. 2928–2936, 2002.
[32] T. R. Rodrıguez and R. Garcıéa, "Theory of Q control in atomic force microscopy," *Applied Physics Letters*, vol. 82, no. 26, pp. 4821–4823, 2003.
[33] S. Gao, L. Chi, S. Lenhert, B. Anczykowski, C. M. Niemeyer, M. Adler, and H. Fuchs, "High-Quality Mapping of DNA-protein Complexes by Dynamic Scanning Force Microscopy," *ChemPhysChem*, vol. 2, no. 6, pp. 384–388, 2001.
[34] D. Ebeling, H. Hölscher, H. Fuchs, B. Anczykowski, and U. D. Schwarz, "Imaging of biomaterials in liquids: a comparison between conventional and Q-controlled amplitude modulation ('tapping mode') atomic force microscopy," *Nanotechnology*, vol. 17, no. 7, p. S221, 2006.
[35] T. De, P. Agarwal, D. R. Sahoo, and M. V. Salapaka, "Real-time detection of probe loss in atomic force microscopy," *Applied Physics Letters*, vol. 89, no. 13, p. 133119, 2006.
[36] N. Kodera, M. Sakashita, and T. Ando, "Dynamic proportional-integral-differential controller for high-speed atomic force microscopy," *Review of Scientific Instruments*, vol. 77, no. 8, p. 083704, 2006.
[37] M. Dukic, J. D. Adams, and G. E. Fantner, "Piezoresistive AFM cantilevers surpassing standard optical beam deflection in low noise topography imaging," *Scientific reports*, vol. 5, p. 16393, 2015.
[38] M. G. Ruppert and S. O. R. Moheimani, "High-bandwidth multimode self-sensing in bimodal atomic force microscopy," *Beilstein journal of nanotechnology*, vol. 7, no. 1, pp. 284–295, 2016.
[39] M. B. Coskun, H. Alemansour, A. G. Fowler, M. Maroufi, and S. O. R. Moheimani, "*Q* Control of an Active AFM Cantilever With Differential Sensing Configuration," *IEEE Transactions on Control Systems Technology*, vol. 27, no. 5, pp. 2271–2278, 2018.

Hazhir Mahmoodi Nasrabadi received his B.Sc. in Electrical Engineering from the University of Tehran, Tehran, Iran in 2018 and honored to be among top 10% students. He is currently a Ph.D. student in Electrical Engineering Department at the University of Texas at Dallas and a member of Laboratory for Dynamics and Control of Nanosystems. His research interests are Electronic, Microfabrication, MEMS, Digital Signal Processing, and Control.

Mohammad Mahdavi received his B.Sc. and M.Sc. degrees in electrical engineering from The University of Tehran, Tehran, Iran, in 2007 and 2010, respectively, and his Ph.D. degree in electrical engineering from The University of Texas at Dallas, TX, USA, in May 2018. He was a Research Scientist with the Department of Systems Engineering at The University of Texas at Dallas. He currently is at Panasonic Corporation of North America as a Senior Product Engineer.

His main research interests involve design, microfabrication and characterization of microelectromechanical systems (MEMS) and sensors.

S. O. Reza Moheimani (Fellow, IEEE) currently holds the James Von Ehr Distinguished Chair in science and technology with the Department of Systems Engineering, The University of Texas at Dallas with appointments in the Electrical and Computer Engineering Department and the Mechanical Engineering Department. His current research interests include the applications of control and estimation in high-precision mechatronic systems, high-speed scanning probe microscopy and atomically precise manufacturing of solid-state quantum devices. He is a fellow of IFAC and the Institute of Physics, U.K. He was a recipient of several awards, including the IFAC Nathaniel B. Nichols Medal and the IEEE Control Systems Technology Award. He is an Editor-in-Chief of Mechatronics.